Title

Progesterone Receptor in the Vascular Endothelium Triggers Physiological Uterine Permeability Preimplantation

Permalink

Journal

ISSN

Authors

Goddard, Lauren M
Murphy, Thomas J
Org, Tönis
et al.

Publication Date

2014

DOI

Peer reviewed

Progesterone Receptor in the Vascular Endothelium Triggers Physiological Uterine Permeability Preimplantation

Lauren M. Goddard,[1] Thomas J. Murphy,[2] Tönis Org,[1] Josephine M. Enciso,[3] Minako K. Hashimoto-Partyka,[1] Carmen M. Warren,[1] Courtney K. Domigan,[1] Austin I. McDonald,[2] Huanhuan He,[4] Lauren A. Sanchez,[1] Nancy C. Allen,[1] Fabrizio Orsenigo,[6] Lily C. Chao,[5] Elisabetta Dejana,[6] Peter Tontonoz,[5] Hanna K.A. Mikkola,[1,2] and M. Luisa Iruela-Arispe[1,2,*]

[1]Department of Molecular, Cell, and Developmental Biology, University of California, Los Angeles, Los Angeles, CA 90095, USA
[2]Molecular Biology Institute, University of California, Los Angeles, Los Angeles, CA 90095, USA
[3]Division of Neonatology, Department of Pediatrics, University of California, Los Angeles, Los Angeles, CA 90095, USA
[4]Department of Human Genetics, University of California, Los Angeles, Los Angeles, CA 90095, USA
[5]Department of Pathology, University of California, Los Angeles, Los Angeles, CA 90095, USA
[6]IFOM, Foundation FIRC Institute of Molecular Oncology, 20139 Milan, Italy
*Correspondence: arispe@mcdb.ucla.edu
http://dx.doi.org/10.1016/j.cell.2013.12.025

SUMMARY

Vascular permeability is frequently associated with inflammation and is triggered by a cohort of secreted permeability factors such as vascular endothelial growth factor (VEGF). Here, we show that the physiological vascular permeability that precedes implantation is directly controlled by progesterone receptor (PR) and is independent of VEGF. Global or endothelial-specific deletion of PR blocks physiological vascular permeability in the uterus, whereas misexpression of PR in the endothelium of other organs results in ectopic vascular leakage. Integration of an endothelial genome-wide transcriptional profile with chromatin immunoprecipitation sequencing revealed that PR induces an *NR4A1* (Nur77/TR3)-dependent transcriptional program that broadly regulates vascular permeability in response to progesterone. Silencing of *NR4A1* blocks PR-mediated permeability responses, indicating a direct link between PR and *NR4A1*. This program triggers concurrent suppression of several junctional proteins and leads to an effective, timely, and venous-specific regulation of vascular barrier function that is critical for embryo implantation.

INTRODUCTION

The endothelium consists of a highly specialized cell population that lines the inner layer of the vascular tree. The particular location of blood vessels imposes functional demands, intrinsic to each organ, that exceed its well-accepted role as a barrier and nonthrombogenic surface. To accommodate organ-specific functions, endothelial cells differ in regard to structure, adhesion molecules, metabolic properties, antigenic expression, and cell-surface determinants (Atkins et al., 2011; Chappell and Bautch, 2010; Regan and Aird, 2012). However, we are significantly behind in our understanding of how unique vascular functions are developed and maintained to confer specific properties to individual tissues.

In the endometrium, cycles of vascular repair and angiogenesis occur in addition to the underlying organ-specific requirements. The repair and regrowth of the endometrium is driven by the sequential and tightly controlled interplay of steroid hormones. In particular, endometrial angiogenesis appears to be regulated by 17-β estradiol (E2), likely through the ER-β receptor, as indicated by its high expression in primate endometrial vascular and perivascular cells (Arnal et al., 2010; Kim and Bender, 2009). Consistent with this prediction, low concentrations of E2 induce proliferative and migratory responses in endothelial cells (Bernelot Moens et al., 2012). More importantly, ER-β knockout mice acquire abnormal vascular function and hypertension associated with endothelial dysfunction and impaired angiogenesis (Iafrati et al., 1997; Zhu et al., 2002). Furthermore, E2 regulates expression of vascular endothelial growth factor (VEGF) and has been shown to promote vascular expansion in the endometrium of primates (Hyder et al., 1996; Sugino et al., 2002).

A unique feature of endometrial vessels is cyclic alterations in vascular permeability. These events result in the recurrent formation of a physiological edema during the second half of the endometrial cycle (secretory phase), a time when progesterone (P4) levels peak (Strauss and Barbieri, 2009). Increased permeability alters the functional endometrium and makes it receptive for embryonic implantation. As part of the decidual response, changes in the degree of permeability parallel the ovarian cycle and are extremely pronounced during pregnancy (Gellersen et al., 2007). The leakage of blood-borne proteins to the interstitium is critical to support the highly metabolic trophoblastic cells

and to ensure the survival of the blastocyst. Interestingly, animals that lack PR are unable to mount a decidual response (Lydon et al., 1996, 1995), placing PR as the upstream coordinator of the cellular and molecular changes that regulate decidualization, including alterations in the stroma, matrix, and vasculature (Large and DeMayo, 2012).

In this study, we provide evidence that PR is required within the endothelial compartment to mediate physiological vascular permeability. The resulting edema is independent of VEGF and instead is triggered by PR-dependent activation of nuclear receptor subfamily, group A, member 1 (NR4A1). Ultimately, through this mechanism, PR is able to selectively target the endometrial vasculature in a coordinated and sustained permeability response.

RESULTS

Complete Deletion of PR Leads to Reduced Physiological Vascular Permeability

To dissect the biological function of PR in the endometrial vasculature, we first examined mice with global deletion of PR (PRKO) and littermate controls. Exposure of control mice to P4 resulted in uterine hyperplasia (Figure 1A) with a concurrent weight increase of 2.5-fold (Figure 1F). In contrast, PRKO uteri failed to mount an equally significant response (Figures 1A and 1F). Sections stained with a collagen IV antibody or perfused intravascularly with *Lycopersicon esculentum* lectin showed equivalent vascular density between groups regardless of whether they were treated with vehicle or hormones (Figures 1B–1D). Histological analysis also revealed a similar overall structure between control and PRKO mice (Figure S1A available online); however, expression of mucin1, an epithelial glycoprotein, and several proteoglycans were decreased in PRKO uteri (Figure S1B). These differences were indicative of deficiencies in the differentiation of the uterus.

Because uterine hyperplasia could be due to increased interstitial fluid, we assessed whether the changes in uterine weight were due to an accumulation of plasma proteins extravasated from the vascular compartment. Hormone (E2 and P4) treatment of control mice resulted in a 3.8-fold increase in Evans blue content. This was in contrast to PRKO mice, which showed no differences in uterine permeability (Figure 1G). Furthermore, inhibition of PR by mifepristone (RU486) blocked the effect of P4 on uterine weight (Figure 1H) and Evans blue extravasation (Figure 1I), whereas inhibitors of other permeability mediators (VEGFR2 [SU11248] and bradykinin [HOE 140]) had no effect. These results suggest that P4, through PR, regulates uterine vascular permeability independently of classical pathological permeability mediators.

PR Expression in the Vasculature Is Restricted to Endothelial Cells of the Veins and Lymphatics of the Uterus and Ovary

Because the endothelium is largely responsible for regulation of vascular permeability, we first evaluated whether the effect of P4 on barrier function is direct and occurs through PR expression in endothelial cells. The presence of PR in the vasculature has been the subject of debate, with a number of publications supporting (Krikun et al., 2005; Maybin and Duncan, 2004; Vázquez et al., 1999) or negating (Ismail et al., 2002; Perrot-Applanat et al., 1995) its expression in endothelial and smooth muscle cells. Using PRLacZ mice (Figure S2), which report both PRA and PRB promoter activation, we found that indeed endothelial cells were β-gal+ (Figure 2A). Interestingly, PR+ endothelial cells were restricted to venules and lymphatics of the uterus and ovary, but absent from arterioles (Figures 2A and S2G). Smooth muscle cells and/or pericytes were also positive; however, β-gal reactivity was equivalent in both arterioles and venules (Figure 2A). Under physiological conditions, PR promoter activity was not detected in the vascular beds of any other organs (Figure S2H), revealing an exclusive organ specificity for PR to vessels of the uterus and ovary.

Expression of PR in the vasculature was confirmed at the protein level by immunohistochemistry. Similar to findings from PRLacZ reporter mice, endothelial cells of veins and lymphatic vessels were positive for both PECAM-1 and PR, whereas arterial endothelial cells lacked PR expression (Figure 2B). Expression of PR in human endometrium was also exclusive to the endothelium of veins (Figure 2C).

It should be emphasized that PR expression in the endothelium is not constitutive. On average, at any given time, PR+ endothelial cells represent 22.7% (32.5% following hormone treatment) of uterine venous and 21% of lymphatic (24% following hormone treatment) endothelial cells per vessel cross-section (Figure 2D). Additionally, on average 30%–40% of uterine vessels express at least one β-gal+ endothelial cell (Figure 2E). Upon pregnancy, transcripts for PR increase by 4.5-fold in the uterus (Figure 2F) and by 3.2-fold in fluorescence-activated cell sorting (FACS)-sorted endothelial cells (Figure 2G). Furthermore, the frequency of PR+ endothelial cells is also increased specifically in veins at day 5.5 of gestation (Figures 2H and 2I).

PR Signaling in the Endothelium Promotes Vascular Permeability In Vivo

To determine whether the effect on vascular permeability was due to PR activity in endothelial cells, we evaluated cell-specific deletion of PR (PR^{ECKO} mice) (Figures S3A and S3B). Cre expression in the uterus and ovary was completely restricted to the endothelium of the vasculature, as determined by β-gal positivity using R26R reporter mice (Figure S3C). The effect of recombination was highly penetrant, as demonstrated by PR deletion in FACS-sorted endothelial cells (Figures S2E and S2F).

Using the Miles assay, we examined control and PR^{ECKO} mice for changes in permeability following hormone treatment (E2+P4). PR^{ECKO} uteri had significantly reduced Evans blue content, yet the duodenum, which lacks PR expression, did not exhibit changes in permeability (Figures 3A and 3B). These results were confirmed by measurements of albumin in the interstitial uterine tissue (Figures 3C and 3D). Whereas hormone-treated control animals exhibited a 4.79-fold increase in albumin levels, PR^{ECKO} mice, albeit responsive, showed only a 1.9-fold increase of no statistical significance (Figure 3C). Albumin levels in PRKO mice were not affected by treatment. It should be stressed that PRKO mice showed greatly reduced levels of proteoglycans (Figure S1B), which have been shown to be important for water retention and likely contribute to explain this effect. As expected, pregnancy increased albumin extravasation in control mice, yet this effect was significantly reduced in PR^{ECKO} mice (Figure 3D).
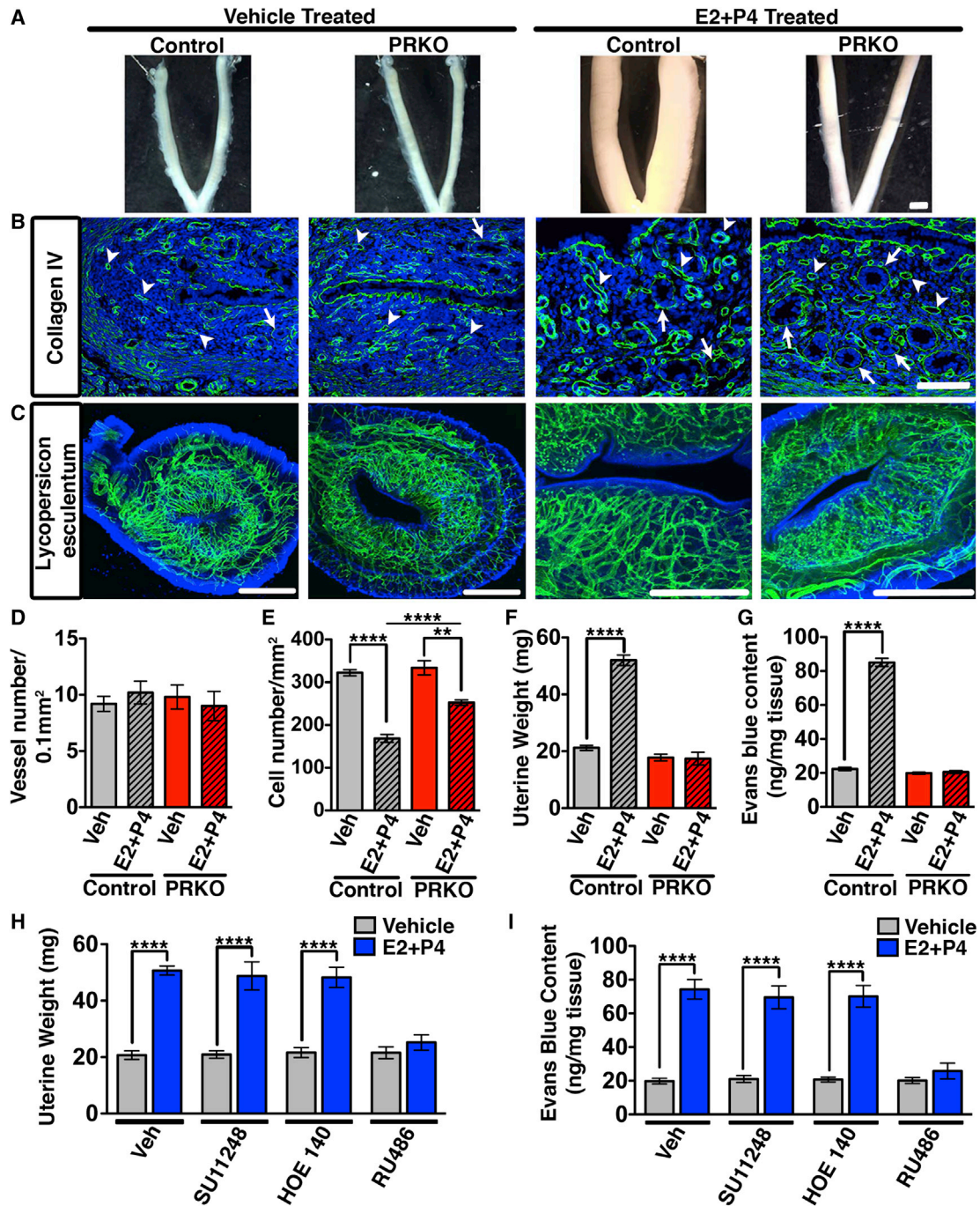
Figure 1. Reduced Physiological Permeability in the Uterus following Global PR Deletion

(A) Effect of hormones (E2+P4) on control (wild-type) and PRKO uteri. Scale bar, 3 mm.

(B) Collagen IV immunostaining (green) detects basement membrane of glands (arrows) and blood vessels (arrowheads). Scale bar, 100 μm.

(C) Uteri following intravascular perfusion with fluorescein isothiocyanate-conjugated *Lycopersicum esculentum* lectin. Scale bar, 1 mm.

(D) Vessel number/0.1 mm^2 in control and PRKO mice.

(E) Uterine cell density/mm^2 in control and PRKO mice.

(F) Uterine wet weight in control and PRKO mice.

(G) Uterine Evans blue content measured by the Miles assay.

(H) Uterine wet weight following concurrent treatment of E2+P4 with inhibitors of VEGFR2 (SU11248), bradykinin (HOE140), and PR (RU486).

(I) Quantification of Evans blue after the conditions listed in (H).

In all panels, error bars show ±SEM. **$p < 0.01$, ****$p < 0.0001$. n = 3–5. See also Figure S1 and Table S1.
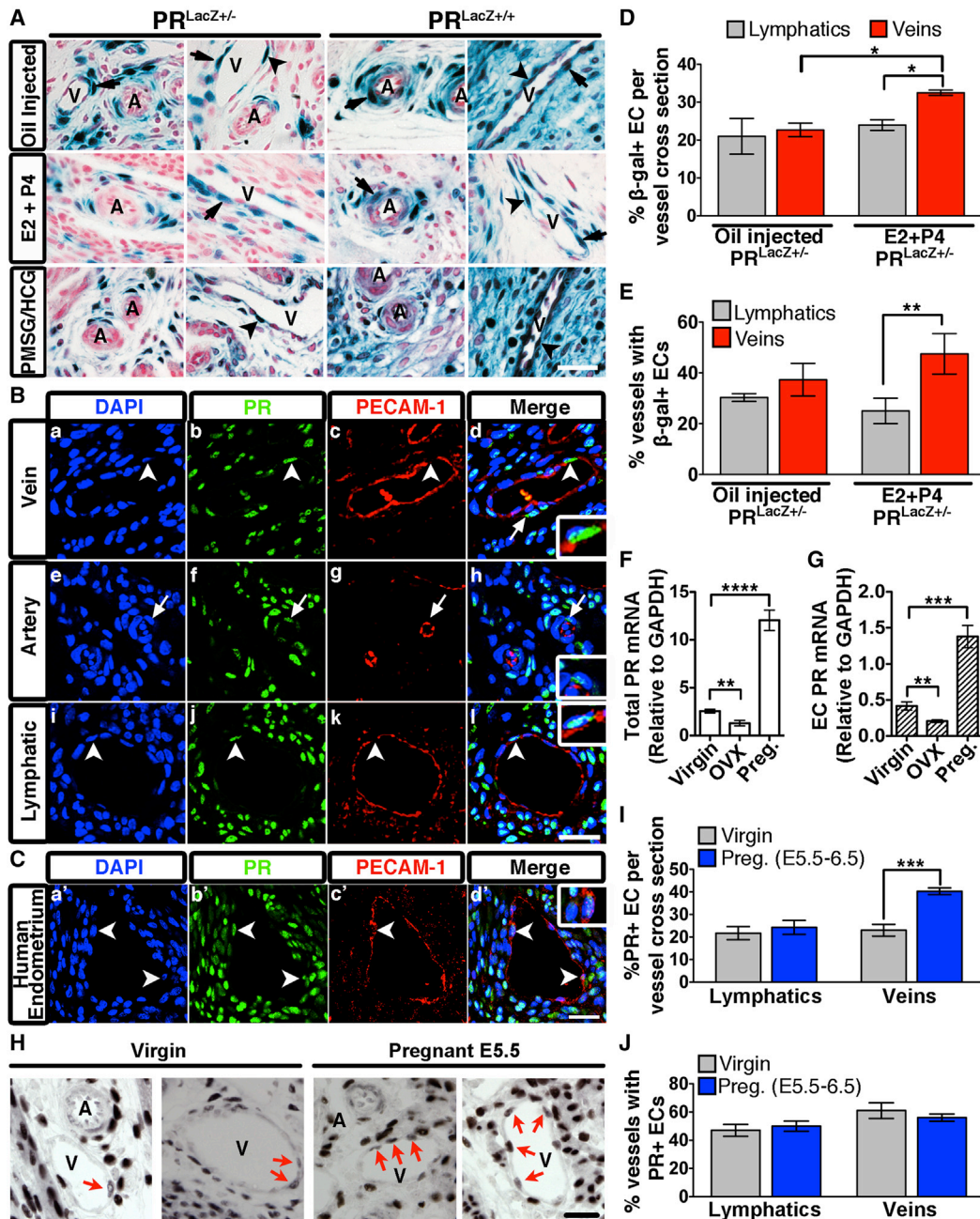
Figure 2. PR Expression in the Murine Vasculature

(A) β-gal positivity in transverse uterine sections from PR$^{LacZ+/-}$ and PR$^{LacZ+/+}$ mice treated with oil, E2 and P4, or pregnant mare serum gonadotropin (PMSG)/human chorionic gonadotropin (HCG). Arrowheads, endothelial cells; arrows, smooth muscle cells; A, arteries; V, veins. Nuclear Fast Red was used as a counterstain.

(B and C) Immunofluorescence of murine (B) and human (C) uterine sections stained for PECAM-1 (red) and PR (green). Nuclei were visualized using DAPI (blue). Arrowheads, endothelial cells; arrows, smooth muscle cells. Insets are higher-magnification images of PR+ endothelial cells.

(D) Percentage of β-gal+ endothelial cells per vessel cross-section from PR$^{LacZ+/-}$ mice (n = 3).

(E) Percentage of vessels in the uterus that contain at least one β-gal+ endothelial cell per cross-section (n = 3).

(F) Total PR mRNA levels in the uterus from virgin, ovariectomized (OVX), and pregnant (E5.5) mice.

(G) PR mRNA levels from isolated uterine endothelial cells from the same mice listed in (F).

(H) PR protein expression in the endothelium of virgin and pregnant (E5.5) mice. Arrows, PR+ endothelial cells; A, arteries; V, veins.

(I) Percentage of PR+ endothelial cells per vessel cross-section from virgin and pregnant uteri (E5.5; n = 3).

(J) Percentage of vessels from virgin and pregnant uteri that contain at least one PR+ endothelial cell per cross-section (n = 3).

In all panels, error bars show ±SEM. Scale bar, 25 μm. *p < 0.05, **p < 0.01, ***p < 0.001 ****p < 0.0001. See also Figure S2.
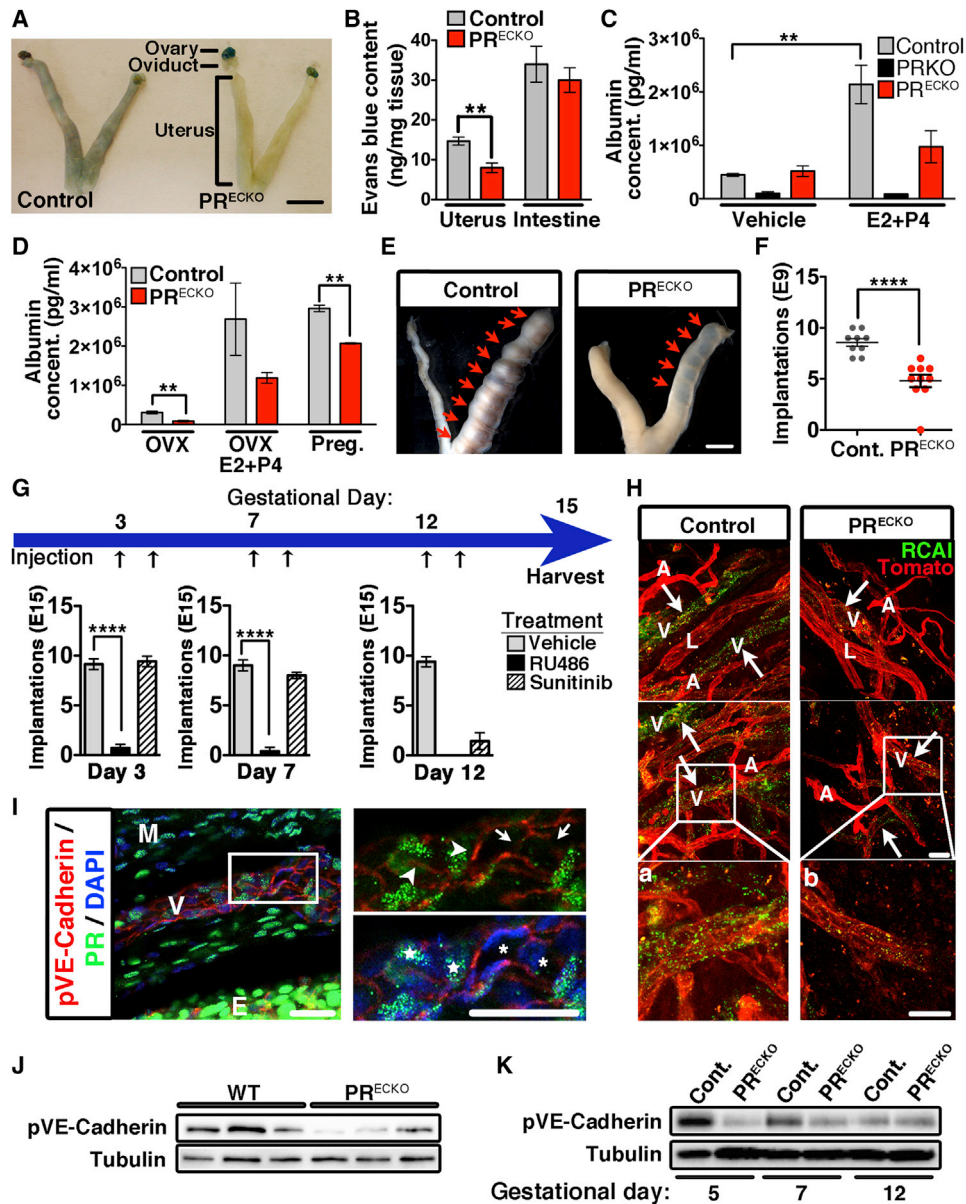
Figure 3. Reduced Vascular Permeability upon Conditional Deletion of PR in the Endothelial Compartment

(A) Evans blue extravasation in control (PRCE; Cre−) and PR^ECKO mice. Scale bar, 7 mm.

(B) Evans blue content in uterus and intestine following hormone stimulation (n = 7–8).

(C) Uterine albumin concentrations from control, PRKO, and PR^ECKO animals following vehicle or E2+P4 treatment.

(D) Uterine albumin concentrations from ovarectomized (OVX) control and PR^ECKO animals following vehicle and E2+P4. Early pregnancy (gestational day 3) was also examined.

(E) Whole-mount images depicting implantation sites (arrows) in control and PR^ECKO mice following embryo transfer. Scale bar, 5 mm.

(F) Quantification of implantation sites at gestational day 9 following embryo transfer in control and PR^ECKO mice.

(G) Schematic depicting treatment of pregnant control females (gestational days 3, 7, and 12) with vehicle, RU486 (PR antagonist), and sunitinib (VEGFR2 antagonist). Black arrows represent time of injection. Implantation sites were quantified at E15 and are represented in the bar graphs below.

(H) *Ricinus communis agglutinin I* (green) and *Lycopersicon esculentum* (red) staining of uteri from control and PR^ECKO animals following E2+P4. Arrows indicate sites of permeability (green). L, lymphatic. (a and b) Enlarged images of boxes in (H). Scale bar, 50 μm.

(I) Immunohistochemistry of pVE-cadherin (red) and PR (green). DAPI (blue) shows nuclei. Higher magnification in box on right. Arrowheads, pVE-cadherin expression; arrows, lack of pVE-cadherin; star, PR+ cell; asterisk, PR− cell; E, endometrium; M, myometrium. Scale bar, 20 μm.

(J) Western blot for pVE-cadherin protein levels in uteri of virgin control and PR^ECKO mice. Tubulin was used as the loading control.

(K) Western blot for total pVE-cadherin protein levels from pregnant uteri (gestational days 5, 7, and 12) of control and PR^ECKO mice. Tubulin was used as the loading control.

In all panels, error bars show ±SEM. **p < 0.01, ****p < 0.0001. See also Figure S3.

To explore the biological relevance of these findings, we performed implantation assays in control and PR^{ECKO} mice (Figure 3E). The results revealed a 43% reduction in the number of implantation sites in PR^{ECKO} mice compared with controls (Figure 3F). Because PR has been shown to regulate VEGF, we sought to evaluate the effect of blocking VEGFR2 during pre- and postimplantation times. P4 blockade, as anticipated, prevented implantation at all gestational time points examined, whereas inhibition of VEGF signaling only impacted embryo viability when administered at postimplantation times (Figure 3G).

The absence of PR in the endothelium did not change vascular density (Figure S3D), but did affect vascular function. Veins specifically failed to exhibit signs of vascular leakage, as shown by injection with *Ricinus communis agglutinin I* (RCAI) lectin (Figure 3H). Phosphorylation of VE-cadherin, a molecular readout of barrier instability, was present at the interface of PR+ cells, while PR− cells showed reduced pVE-cadherin (Figure 3I). This finding was also confirmed by total protein lysates from uteri of control and PR^{ECKO} mice (Figure 3J). Finally, whereas permeability associated with pregnancy resulted in an increase in VE-cadherin phosphorylation, this effect was muted in PR^{ECKO} mice (Figure 3K).

We further scrutinized the function of PR in endothelial cells by ectopic expression using a transgenic mouse model (Figure S3G; Table S1). The relative levels of transgenic PR protein confirmed that the lung was by far the site of highest expression, followed by the intestine, whereas the kidney, uterus, and heart showed a complete absence of PR (Figures S3H–S3J). Consistent with the lack of transgene expression in uteri, P4 treatment resulted in equivalent extravasation of Evans blue (Figure S3K). In contrast, vascular permeability in PRTg lungs was 5.3-fold greater than baseline, and leakage in the duodenum increased by 1.6-fold (Figures S3L and S3M). Immunohistochemical analysis of RCAI-injected mice revealed barrier dysfunction in the lung following hormone treatment and provided additional support to the Miles assay (Figure S3N).

PR Activation in Endothelial Cells Results in Interendothelial Gaps and Decreased Endothelial Monolayer Resistance

Having established that endothelial PR promoted vascular permeability in vivo, we returned to in vitro settings to gain mechanistic insights. First, we examined human endometrial endothelial cells (HEECs) that express endogenous PR. Similar to the findings in murine and human endometrial sections, the presence of PR was heterogeneous (Figure 4A), which provided an important advantage because it allowed for concurrent assessment of PR− cells in the same culture. To determine the effect of P4 on junctional complexes, we used β-catenin immunolocalization. Cell-cell integrity was stable in nontreated (Figure 4Aa) and vehicle-treated (Figure 4Ab) HEECs. However, P4 treatment induced translocation of β-catenin away from adherens junctions and resulted in the formation of intercellular gaps only in HEECs expressing PR (orange nuclei), while cells that lacked PR remained bound (Figure 4Ac, bracket).

A more comprehensive evaluation of the effect of PR on junctional proteins was performed in human umbilical vein endothelial cells (HUVECs) infected with a PR lentivirus (Figures 4B and 4C). Exposure to P4 resulted in clear loss of PECAM-1 (Fig-

ure 4B), VE-cadherin (Figure S4A), and β-catenin cell-surface expression (Figure 4C). Biochemically, β-catenin was found to translocate from the cell membrane to the cytosol and nucleus upon treatment with P4 (Figures 4C and 4D). These effects were absent in HUVECs that lacked PR whether in the presence or absence of P4 (Figure S4B).

To evaluate the progression of junctional breakdown in real time, we used electrical cell-substrate impedance sensing (ECIS) on endothelial monolayers (Figure 4E). Following P4 treatment, human dermal endothelial cells (HDECs) overexpressing PR exhibited a progressive decrease in resistance, with initial barrier destabilization occurring between 4 and 8 hr after P4 addition (Figure 4F). At 17 hr, the reduction in barrier resistance was equivalent to that induced by thrombin (at 30 min), a landmark control for these types of experiments. Notably, in contrast to the short effect mediated by thrombin, P4 exposure resulted in persistent and continuous barrier breakdown.

To confirm that the changes in resistance were due to cellular gaps, we visualized β-catenin expression in the same cells measured by ECIS. As expected, cells that exhibited a decrease in electrical resistance also displayed discontinuous cell-cell adhesion (Figure S4C). Furthermore, the effects on barrier integrity were found to be dose dependent (Figure 4G) and ceased after removal of P4 (at physiological levels) (Figure 4H). Surprisingly, inhibition of classical permeability signaling molecules, including Src (Figure S4D), PI3K (Figure S4E), ROCK (Figure S4G), and VEGFR2 (Figure S4H), or taxol-mediated microtubule stabilization (Figure S4F) did not inhibit P4-induced permeability, suggesting that a novel mechanism may act downstream of PR.

Endothelial PR Signaling Alters Junctional Protein Expression

Using next-generation RNA sequencing (RNA-seq), we explored the notion that PR signaling may transcriptionally alter the expression of endothelial junctional proteins. Following 4 hr of P4 treatment, we compared the fold change of several genes known to regulate vascular permeability (Figure 5A). As expected, many of the genes that encode proteins important for junctional stability, such as VE-cadherin (*CDH5*), VE-PTP (*PTPRB*), PECAM-1, and claudin-5 (*CLDN5*), were reduced upon P4 exposure. Quantitative PCR (qPCR) analysis of VE-cadherin and claudin-5 confirmed the reduction noted by RNA-seq (Figure 5B). Western blot analysis demonstrated a significant reduction in junctional protein levels starting at 16 hr after treatment (Figures 5C and 5D), supporting the kinetics revealed by HUVEC immunofluorescence (Figure S4A). β-catenin levels remained unchanged at both the RNA and protein levels, which correlated with protein translocation rather than reduction. Other endothelial-matrix associated proteins, including focal adhesion kinase (FAK) and β1-integrin, were not affected by P4 addition (Figure S5A).

To determine whether transcriptional activation and subsequent protein synthesis were required for P4-mediated permeability, HUVECs were treated with inhibitors of transcription and translation (Figures 5E and 5F). Both inhibitors completely blocked the decrease in monolayer resistance observed upon P4 treatment, confirming the requirement for transcriptional
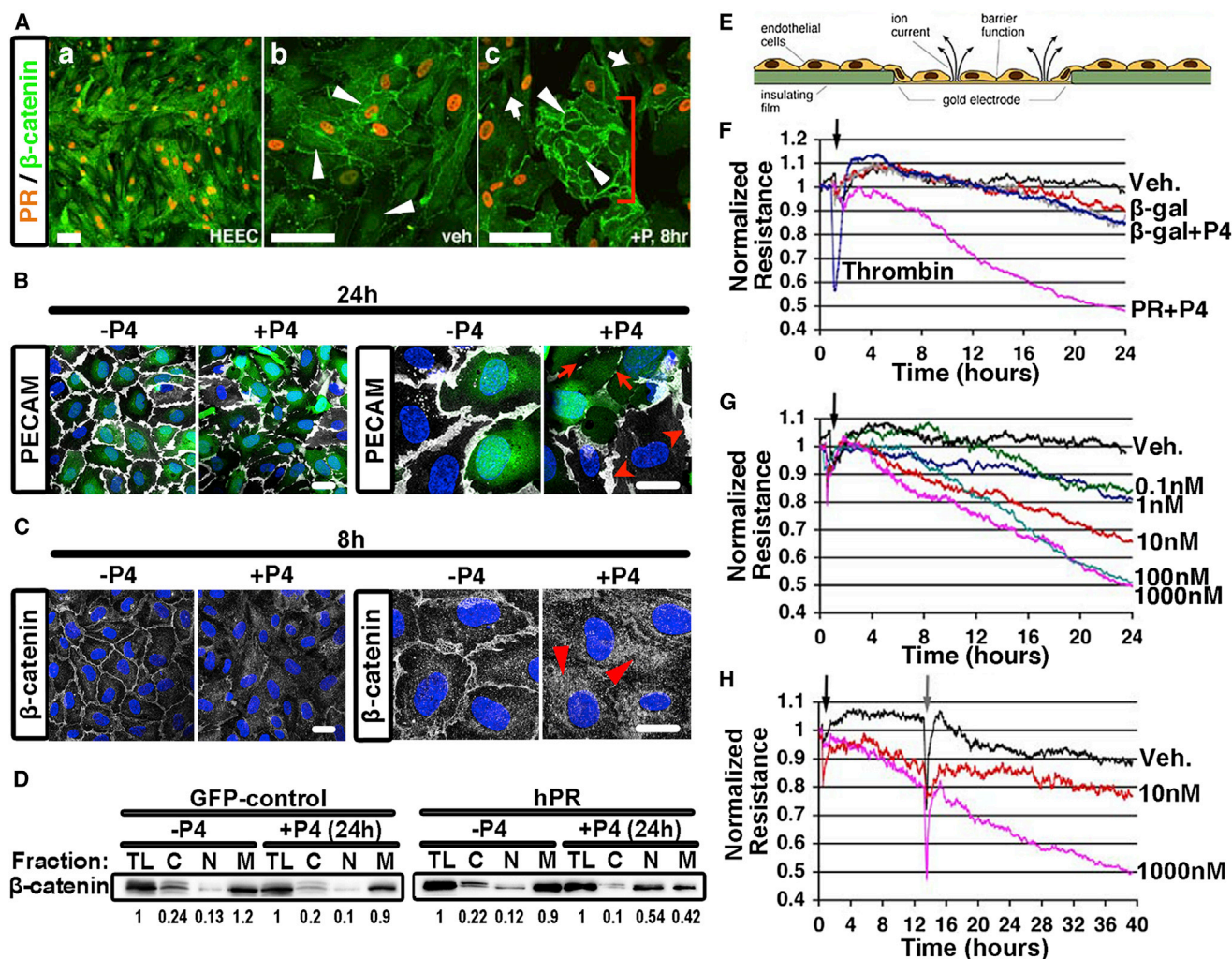
Figure 4. PR Activation in Endothelial Cells Results in Barrier Disruption

(A) Immunohistochemistry of HEEC for PR (orange) and β-catenin (green, arrows). (a) low magnification, (b) high magnification treated with vehicle, and (c) high magnification treated with P4. PR− cell islands are indicated by the bracket. Scale bar, 100 μm.

(B) PECAM (white) in HUVECs infected with a PR lentivirus (GFP, green) following 24 hr of P4 treatment (100 nM). DAPI (blue) shows nuclei. Arrows indicate junctional disruption. Arrowheads show the presence of PECAM in PR− cells. Scale bar, 10 μm.

(C) β-catenin (white) in HUVECs infected with a PR lentivirus (green, GFP) following 8 hr of P4 treatment (100 nM). DAPI (blue) shows nuclei. Arrowheads show translocation of β-catenin from the cell membrane to cytosol. Scale bar, 10 μm.

(D) Presence of β-catenin in subcellular fractions from HUVECs infected with GFP-control or hPR lentivirus. Cells were treated with or without P4 for 24 hr as indicated. C, cytosol; N, nuclear; M, membrane; TL, total lysate. Numbers below indicate quantification of western blot.

(E) Diagram depicting ECIS.

(F) Monolayer resistance of HDECs following infection with a PR adenovirus and β-gal control construct. Thrombin was used as positive control.

(G) HDEC monolayer resistance following treatment with increasing concentrations of P4 as indicated.

(H) Evaluation of HDEC monolayer resistance after removal of P4 from the media. Black arrow, P4 addition; gray arrow, P4 removal. n = 3–5.
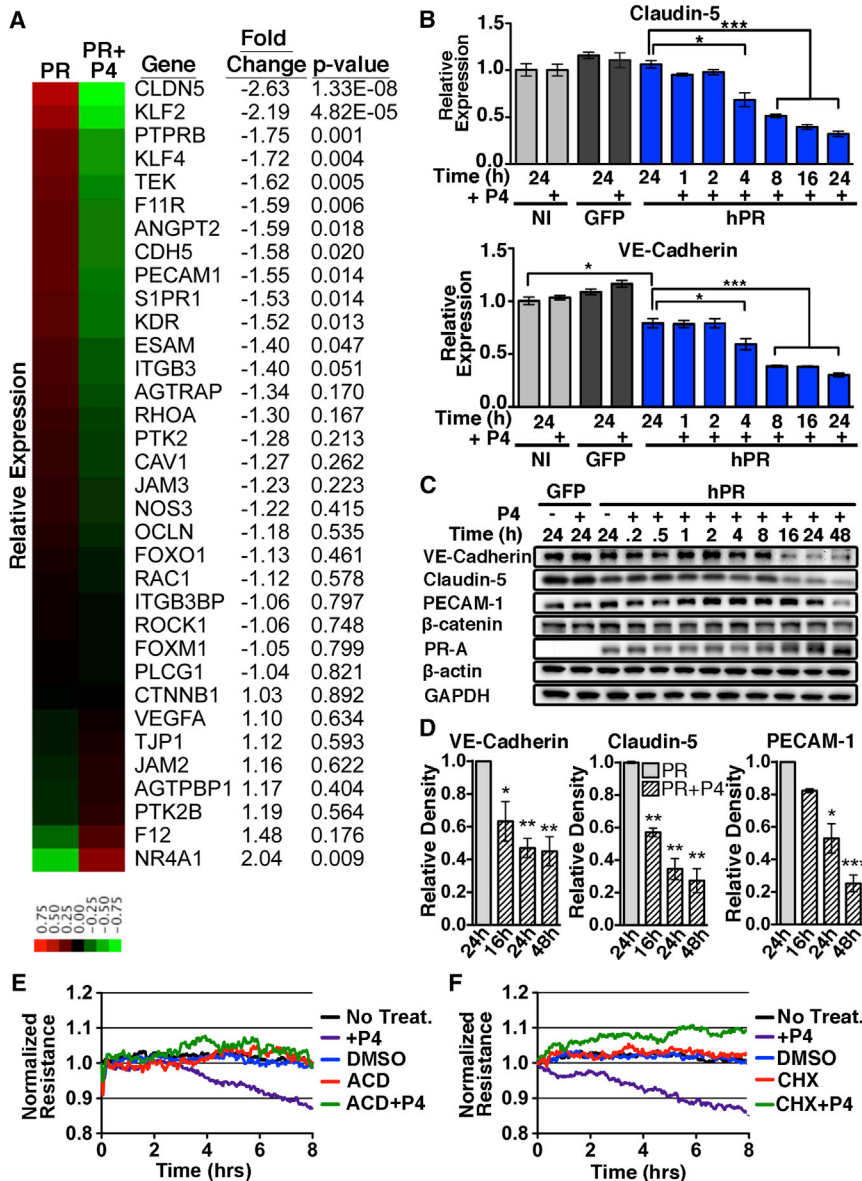
See also Figure S4.

regulation and de novo protein synthesis downstream of PR signaling.

PR Binds Directly to the *NR4A1* Promoter and Regulates *NR4A1* Gene Expression

A concrete elucidation of PR's mechanism of action required us to ascertain the cohort of PR-regulated genes in the endothelium and identify within this cohort the intermediate effector(s). For this purpose, we obtained a global readout of PR-binding sites in the HUVEC genome using chromatin immunoprecipitation sequencing (ChIP-seq). In the absence of ligand (PR only), we resolved 525 PR-binding sites, whereas activation of the receptor by P4 (PR+P4) resulted in a much higher number of PR-binding sites (9,906), 396 of which overlapped with PR only peaks. To identify genes that might be regulated by PR, we next associated PR+P4-binding sites

A

		Gene	Fold Change	p-value
PR	PR+P4	CLDN5	-2.63	1.33E-08
		KLF2	-2.19	4.82E-05
		PTPRB	-1.75	0.001
		KLF4	-1.72	0.004
		TEK	-1.62	0.005
		F11R	-1.59	0.006
		ANGPT2	-1.59	0.018
		CDH5	-1.58	0.020
		PECAM1	-1.55	0.014
		S1PR1	-1.53	0.014
		KDR	-1.52	0.013
		ESAM	-1.40	0.047
		ITGB3	-1.40	0.051
		AGTRAP	-1.34	0.170
		RHOA	-1.30	0.167
		PTK2	-1.28	0.213
		CAV1	-1.27	0.262
		JAM3	-1.23	0.223
		NOS3	-1.22	0.415
		OCLN	-1.18	0.535
		FOXO1	-1.13	0.461
		RAC1	-1.12	0.578
		ITGB3BP	-1.06	0.797
		ROCK1	-1.06	0.748
		FOXM1	-1.05	0.799
		PLCG1	-1.04	0.821
		CTNNB1	1.03	0.892
		VEGFA	1.10	0.634
		TJP1	1.12	0.593
		JAM2	1.16	0.622
		AGTPBP1	1.17	0.404
		PTK2B	1.19	0.564
		F12	1.48	0.176
		NR4A1	2.04	0.009

Relative Expression

0.75 0.50 0.25 0.00 -0.25 -0.50 -0.75

B

Claudin-5

VE-Cadherin

C

GFP / hPR

D

VE-Cadherin Claudin-5 PECAM-1

E

F

Figure 5. PR Activation Leads to Changes in Expression of Junctional Proteins

(A) Heatmap representing the relative expression and fold change of genes known to regulate vascular permeability in PR versus PR+P4 HUVECS at 4 hr.

(B) qPCR of VE-cadherin (*CDH5*) and claudin-5 (*CLDN5*) expression following P4 treatment of noninfected (NI), GFP-infected (GFP), and PR-infected (hPR) HUVECs. n = 3. GFP-infected HUVECs were used as a control for infection.

(C) Western blot analysis of total protein levels from GFP control or PR-infected HUVECs following P4 treatment. Glyceraldehyde 3-phosphate dehydrogenase (GAPDH)/β-actin served as loading controls. Blots are representative of three independent experiments.

(D) Densitometry of VE-cadherin, claudin-5, and PECAM-1 protein levels following P4 treatment. n = 3.

(E and F) Evaluation of HUVEC monolayer resistance following treatment with cycloheximide (CHX, 10 μg/ml), actinomycin D (ACD, 10 μg/ml), or P4 and vehicle as indicated.

Error bars show ±SEM. *p < 0.05, **p < 0.01, ***p < 0.001. See also Figure S5.

(9,906) with nearby genes within a 50 kb range from transcriptional start sites, and identified 3,886 predicted bound genes following P4 treatment (Figure 6A).

To find direct PR target genes whose expression was affected in response to P4, it was necessary to combine the ChIP-seq and RNA-seq data sets (Figure 6B). RNA-seq analysis of HUVECs yielded 406 upregulated and 431 downregulated genes with a p value less than 0.01 (Figure 6B). These genes were then intersected with the list of 3,886 genes predicted to be regulated by the PR-binding sites obtained from ChIP-seq evaluation. This analysis showed that 93 (23%) of activated and 214 (49%) of repressed genes are likely direct targets of PR in endothelium. To identify which biological processes might be regulated by PR, we subjected directly activated (Figure 6C) and repressed (Table S2) gene lists to the DAVID Bioinformatics Database for Gene Ontology (GO) (Huang et al., 2009). Interestingly, "transcription" was the top term associated with directly upregulated genes (Figure 6C). Since P4-mediated permeability requires de novo protein synthesis, we further focused on the 28 transcription factors that are directly upregulated by PR by examining fold upregulation after P4 treatment (Figure 6D).

Notably, only one of these transcription factors, *NR4A1*, has been previously implicated in vascular permeability (Zhao et al., 2011). Two distinct PR-binding peaks were found between 10 and 25 kb upstream of the *NR4A1* start site in PR+P4 samples, but not in respective controls (Figure 6E). qPCR confirmed significant *NR4A1* upregulation as early as 1 hr after P4 addition (Figure 6F). Interestingly, *NR4A1* expression continued to increase and sustained elevated levels as long as 24 hr after P4 stimulation. To further validate direct PR binding at the *NR4A1* locus, we analyzed intervals that putatively contained PR binding, along with a negative control region, by ChIP-qPCR (Figure 6G). PR binding was significantly enriched at both regions corresponding to ChIP-seq peaks as compared with control samples (Figure 6G).

NR4A1 Is Required for Progesterone-Mediated Endothelial Permeability

Endothelial barrier stability was enhanced when *NR4A1* was knocked down using small interfering RNA (siRNA; Figures 7A
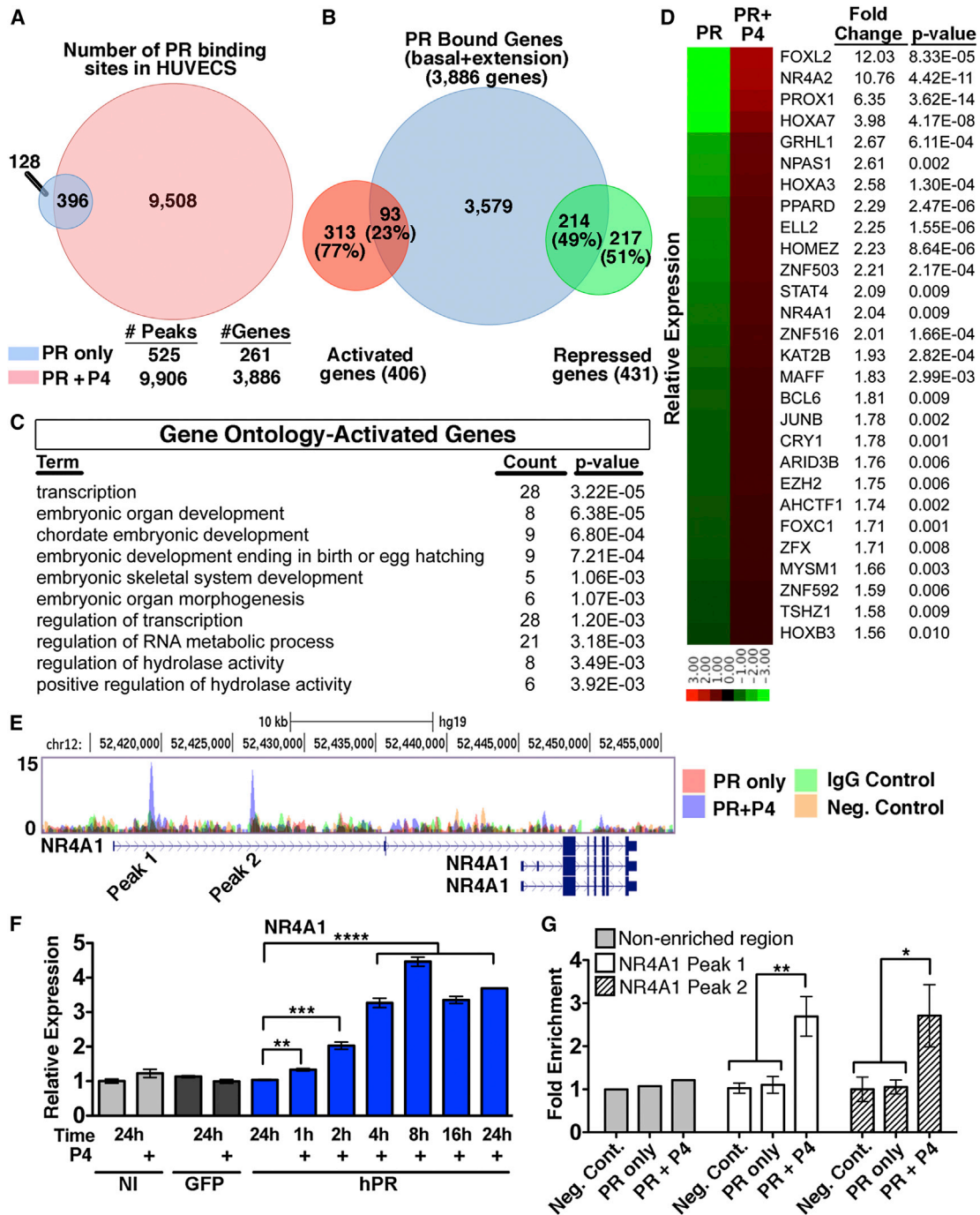
Figure 6. *NR4A1* Is a Direct Target of PR

(A) Venn diagram of PR binding peaks between HUVECs treated with (red) or without (blue) P4 for 1h. Predicted gene numbers based on analysis of binding peaks within 50kb of the transcriptional start site.

(B) Venn Diagram representing the overlap between genes predicted to be regulated by PR by ChIP-seq and genes with a p value less than 0.01 as determined by RNA-seq.

(C) Top gene ontology terms from activated genes bound by PR as predicted by DAVID.

(D) Heat map depicting expression and fold change of the 28 transcription factors that were in the top gene ontology pathway from (C).

(E) Depiction of two PR binding peaks upstream of the *NR4A1* gene in the presence of P4. Neg. control = noninfected (NI) HUVECs.

(F) qPCR analysis of *NR4A1* expression following P4 treatment of noninfected (NI), GFP infected (GFP) and PR infected (hPR). n = 3.

(G) ChIP-qPCR analysis of both *NR4A1* binding peaks following P4 treatment. *p < 0.05, **p < 0.01, ***p < 0.001, ****p < 0.0001.

In all panels, error bars show ±SEM. See also Figure S6 and Table S2.
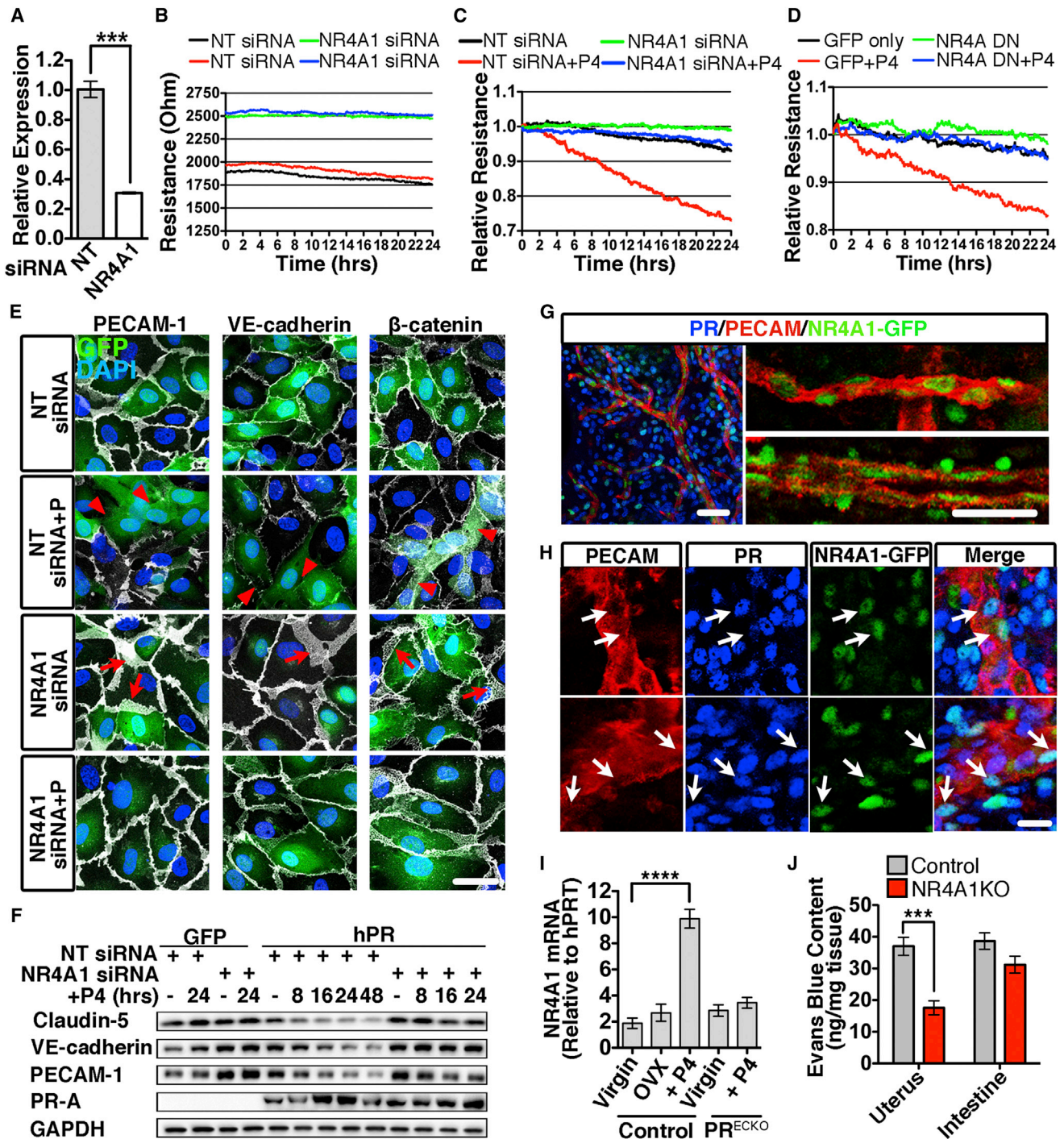
Figure 7. Knockdown of *NR4A1* Inhibits Progesterone-Mediated Permeability

(A) qPCR analysis of *NR4A1* following transfection of HUVECs with either nontargeting (NT) or *NR4A1* siRNA. n = 3.

(B) Baseline HUVEC monolayer resistance following *NR4A1* knockdown.

(C) HUVEC monolayer resistance after transfection with *NR4A1* or NT siRNA in the presence of P4.

(D) HUVEC monolayer resistance following adenoviral infection with a NR4A family dominant-negative (NR4A DN) and control (GFP) in the presence of P4.

(E) HUVECs expressing PR (GFP, green) and transfected with either NT or *NR4A1* siRNA were treated with P4 for 24 hr. PECAM, VE-cadherin, and β-catenin (white) were used to visualize junctions. DAPI (blue) denotes nuclei. Arrowheads indicate a reduction in junctional proteins. Arrows show expanded junctional area. Scale bar, 50 μm.

(F) Junctional proteins from GFP or PR infected HUVECs following transfection with either NT or *NR4A1* siRNA followed by P4 treatment. GAPDH was the loading control.

(legend continued on next page)

and 7B). Although P4 increased permeability in PR-expressing HUVECs, this effect was largely blocked by the knockdown of *NR4A1* (Figure 7C). To further scrutinize these findings, we infected HUVECs with an adenovirus containing a dominant-negative construct (NR4A DN) for all NR4A family members (Pei et al., 2006). Similar to *NR4A1* knockdown, overexpression of the NR4A DN inhibited P4-mediated permeability (Figure 7D).

Immunocytochemistry further supported the concept that *NR4A1* acts downstream of PR to regulate barrier breakdown in endothelial cells. Although HUVECS treated with nontargeting siRNA showed reduced VE-cadherin and PECAM-1 levels as well as β-catenin relocalization, these effects were blocked in cells with *NR4A1* knocked down (Figure 7E). Interestingly, knockdown of *NR4A1* led to an increase in membrane expression of all three junctional proteins, consistent with the increase in basal resistance revealed by ECIS. Protein analysis further demonstrated the reduction of claudin-5, PECAM-1, and VE-cadherin in HUVECs transfected with nontargeting siRNA (Figures 7F and S7A–S7C). PR levels between nontargeting and knockdown cells were similar, ruling out possible changes in PR expression as the determinant of this effect.

Since PR also directly stimulates *NR4A2* expression (Figures S6A–S6C), we examined the effect of *NR4A2* reduction on permeability (Figure S6D). Knockdown of *NR4A2* by three independent siRNA constructs did not inhibit P4-mediated permeability, demonstrating a unique role for *NR4A1* in the regulation of the endothelial barrier (Figure S6E).

We examined the in vivo expression of *NR4A1* using a GFP reporter mouse (Table S1). GFP, as a readout of *NR4A1*, was largely restricted to the vasculature, particularly endothelial cells (Figure 7G). Unlike PR expression, *NR4A1* was seen in both veins and arteries, but colocalization of PR and *NR4A1* was frequently found in veins (Figure 7H). Using qPCR of whole uteri, we found that *NR4A1* expression was responsive to P4 stimulation, as mRNA levels were 3.8-fold higher following treatment. This same increase was not seen in PR^ECKO^ mice, suggesting that PR signaling in the endothelium enhances *NR4A1* expression (Figure 7I). To determine whether loss of *NR4A1* had biological implications for uterine vascular permeability, we examined Evans blue extravasation following hormone stimulation in *NR4A1* null mice. Similar to findings in PR^ECKO^ mice, a significant reduction in Evans blue content was seen in the uterus, but not the intestine, of *NR4A1* KO mice (Figure 7J).

The ability of *NR4A1* to directly control expression of junctional proteins was also tested in gain-of-function experiments. Overexpression of *NR4A1* resulted in a marked reduction in VE-cadherin, claudin-5, and PECAM-1 in the absence of P4 (Figure S7E). Furthermore, expression of *NR4A1* alone increased monolayer resistance as determined by ECIS (Figure S7D), providing additional functional validation. These results indicate that *NR4A1* is

required and acts downstream of PR to mediate endothelial specific vascular permeability.

DISCUSSION

The sequential and highly coordinated actions of the steroid hormones E2 and P4 are known to regulate epithelial and stromal functions in the endometrium (Das et al., 2009; Gellersen et al., 2007; Wetendorf and DeMayo, 2012). Changes imposed by these steroid hormones prepare the endometrium for implantation and continue to be essential during the subsequent postimplantation phases to ensure a successful pregnancy (Franco et al., 2012; Wetendorf and DeMayo, 2012). Whereas much is known about the molecular and cellular events that occur downstream of epithelial and stromal responses, the unique series of changes that are imposed on the uterine vasculature before, during, and after implantation are only known at the level of morphological description. Here, we show that PR within the endothelium is responsible for initiating a series of events that lead to physiological edema in the endometrium. Specifically, PR induces expression of the orphan nuclear receptor *NR4A1*, which in turn destabilizes the endothelial barrier function within PR-expressing endothelial cells. The consequence is restricted and sustained vascular permeability directed by circulating P4.

The contribution of P4 as the chief regulator of vascular alterations during the secretory phase was implied by earlier observations that mice that lacked PR failed to mount a decidual response (Lydon et al., 1995, 1996). Because expression of PR in the endothelium was not constitutive, we believed that the effect on vessels was triggered through the secondary action of permeability modulators. An obvious culprit, VEGF, has frequently been suggested to be responsible for the cycle of vascular changes in the uterus. In fact, VEGF is induced by steroid hormones (Hyder et al., 1996; Shifren et al., 1996; Sugino et al., 2002) and pharmacological blockade of this growth factor in primates impairs endothelial repair and angiogenic growth (Fan et al., 2008). Surprisingly, we found that blockade of VEGF does not prevent the physiological edema that occurs prior to implantation; instead, these events appear to be triggered by P4-driven mechanisms that are independent of VEGF. These findings pointed to either alternative permeability mediators or a direct role of PR in the endothelium. It should be noted, however, that inactivation of VEGF signaling postimplantation, like P4 blockade, impacts both permeability and embryo viability. Thus, it appears that the mechanisms that regulate permeability responses pre- and postimplantation are likely distinct.

To evaluate the contribution of PR in the vascular endothelium, we adopted loss- and gain-of-function approaches. Although mice that lacked PR in the endothelium were able to host the typical decidual response by stromal cells, they showed an

(G) *NR4A1* (GFP, green) localization in the vascular endothelium in vivo (PECAM, red). Scale bar, 25 μm.

(H) PR (blue) and *NR4A1* (GFP, green) colocalization in uterine vasculature (PECAM, red). Arrows indicate endothelial cells with *NR4A1* and PR. Scale bar, 20 μm.

(I) qPCR of *NR4A1* from the uteri of virgin, ovariectomized (OVX), and PR^ECKO^ mice treated with or without P4. n = 3.

(J) Evans blue content from the uterus and intestine following hormone stimulation of control (wild-type) and *NR4A1*KO mice. ***p < 0.001, ****p < 0.0001. Error bars show ±SEM.

See also Figure S7.

impaired ability to mount a physiological edema response, with consequences for implantation. In contrast, transgenic animals that misexpressed PR on endothelial cells in organs other than the uterus displayed an acute permeability response upon ligand exposure. Together, these findings implicated P4 as the mediator of the permeability responses in the uterus.

How does P4 drive vascular permeability? Although the molecular mechanisms of P4's action via binding to its receptor are well established (Edwards et al., 1995; McKenna and O'Malley, 2000; Rubel et al., 2012), the effects of this hormone on endothelial cells have not been explored at the molecular level. An evaluation of the literature on the effect of PR in epithelial cells was not informative as to how this transcription factor could promote destabilization of barrier function in endothelial cells. Furthermore, our in vitro experiments indicated that the effect of PR on endothelial permeability required transcriptional control. Following that lead, we performed global transcriptional profiling (RNA-seq) of endothelial cells treated with P4. These data initially failed to provide insights into the process whereby PR promotes permeability. It was only by integrating ChIP-seq analysis with the transcriptional profile that we were able to identify *NR4A1* as the possible link.

The orphan nuclear receptor *NR4A1* is a member of the NR4A transcription factor family, which is expressed by a broad number of cell types. The effects mediated by *NR4A1* are pleiotropic and cell-type dependent, and impact metabolism, homeostasis, and inflammation (Pearen and Muscat, 2010; Zhao and Bruemmer, 2010). Recently, *NR4A1* was also shown to be expressed by endothelial cells and to induce pathological permeability responses (Zhao et al., 2011). Reports indicating that *NR4A1* plays a role in permeability also raised the possibility that this molecule might be downstream of PR signaling.

A hallmark of vascular leakage is the formation of intercellular gaps via disruption of cell-cell contacts resulting in a loss of barrier integrity (Dejana et al., 2008; Dvorak, 2010; Komarova and Malik, 2010). Along these lines, endothelial cells expressing PR showed disruption of cell-cell interactions upon exposure to the ligand. Interestingly, silencing of *NR4A1* in cells expressing PR and treated with the ligand blocked the effect of P4 on permeability. These findings clearly indicated that PR was upstream of *NR4A1* in the control of endothelial barrier function. Furthermore, we found that *NR4A1* coordinates an effective program of repression of junctional proteins, including VE-cadherin, claudin-5, and PECAM1.

Our results indicate that under homeostatic conditions, PR is highly restricted to uterine blood vessels, at the exclusion of vessels from other organs. Interestingly, expression of PR is selective to veins and lymphatic vessels. Endothelium from arteries conspicuously lacks PR, whereas high expression is noted in the smooth muscle layer of these vessels. This exquisite specificity enables local and controlled functions to be triggered by a systemically distributed ligand.

Is PR the only regulator of permeability in the uterus? That is unlikely, but our findings would indicate that removal of this receptor from the endothelium significantly impacts permeability and implantation. This is in sharp contrast to VEGF blockade, for example, which did not impact embryo viability at preimplantation times. Another important point is that genomic inactivation

of PR completely blocks permeability. Initially, this finding led us to speculate that PR might regulate permeability through its actions in other cell types. However, comparisons between global and cell-specific PRs are confounded by the global impact of PR on the differentiation of the uterus. In fact, deletion of PR from the onset of development impacts the differentiation of uterine epithelium and stroma, including a reduction in proteoglycan levels (Figure S1B) that are critical for interstitial water retention and contribute to regulation of fluid trafficking in tissues. This might explain why PRKO mice exhibit a much lower basal content of albumin, while control and PR^ECKO mice are equivalent at baseline and only differ upon hormonal treatment.

The findings presented here are in accordance with and further explain the uterine vascular fragility experienced by users of long-term progestin-only contraceptives (Hickey and Fraser, 2002; Kovacs, 1996; Shoupe et al., 1991). In fact, prolonged exposure to progestins results in abnormal endometrial bleeding despite increased levels of tissue factor expression (Runic et al., 2000).

Structural and molecular differences in the endothelium of distinct tissues reflect its role in meeting the diverse requirements of individual organ sites. The recurrent cycles of physiological permeability in the endometrium are unique to this tissue and must be regulated in a timely manner. Here, we have shown that this physiological permeability requires a molecular toolkit distinct from that of pathological permeability. Taken together, our findings highlight the process by which endothelial cells detect and respond to systemic hormones to trigger local, timely, and effective changes in barrier function.

EXPERIMENTAL PROCEDURES

Mouse Models

Details about the mouse models and genotyping used can be found in the Extended Experimental Procedures. All animals were housed in a pathogen-free environment in an AAALAC-approved vivarium at UCLA, and experiments were performed in accordance with the guidelines of the Committee for Animal Research.

Hormone Treatment

Female tie1-PRTg, PRLacZ, PR^ECKO, PRKO, and *NR4A1*KO mice and littermate controls (8–12 weeks old) were treated with hormones as previously described (Lydon et al., 1995). Details on the hormone treatments can be found in the Extended Experimental Procedures.

Vascular Permeability Assays

Following hormone treatment, mice were injected intravenously (i.v.) with either Evans blue dye (Miles assay; 1 ml/kg of 3% Evans blue) or select lectins and allowed to circulate for 20 min before perfusion fixation (1% paraformaldehyde). Select organs were removed, blotted dry, and weighed (wet weight). Evans blue was extracted from tissues with formamide overnight at 55°C and measured in duplicate by a spectrometer at 620 nm. Details on extraction and quantification of albumin are provided in the Extended Experimental Procedures.

Embryo Isolation and Implantation

Embryos were obtained from wild-type females mated with fertile males. Embryos (2- to 4-cell stage) were recovered by flushing the uteri with Hank's balanced salt solution. Twelve embryos were transferred into anesthetized pseudopregnant females via the infundibulum into the ipsilateral ampulla of the uterine tube. The peritoneum was sutured and the skin was closed with a clamp. Counts of implantation sites were performed using a dissecting

microscope (Leica Microsystems) and image acquisition and analytic software (SPOT Imaging Solutions).

Immunohistochemistry

Tissue (5 μm) and/or vibratome (300 μm) sections were immunostained with antibodies against PR (SP2; Lab Vision), PECAM-1 (MEC 13.1; BD Biosciences), and GFP (Abcam). Antigen retrieval using Tris-EDTA (pH 9.0) was required for PR staining of formalin-embedded tissues. Alexa Fluor secondary antibodies were used to recognize primary antibodies (Molecular Probes/Life Technologies). Sections were analyzed using a Zeiss LSM 510 META multiphoton microscope with built-in Axiocam and acquired using Zen software (Zeiss). Details of β-galactosidase staining can be found in the Extended Experimental Procedures.

Immunoblotting and Immunoprecipitation

Proteins were resolved by SDS-PAGE, transferred to nitrocellulose (BA-S 83; Optitran), and incubated overnight with antibodies against PR (SP2; Lab Vision), VE-cadherin (Cell Signaling), PECAM-1 (Cell Signaling), claudin-5 (Invitrogen), β-catenin (Sigma), β-actin (Sigma), pVE-cadherin (pY685 [Orsenigo et al., 2012]), FAK (BD Biosciences), β1-integrin (AB1952; Millipore) and myc (Cell Signaling). Blots were incubated with horseradish peroxidase-conjugated secondary antibodies (Bio-Rad Laboratories), developed with Supersignal West Pico Chemiluminescent Substrate (Thermo Scientific), and imaged with the use of the Bio-Rad ChemiDoc XRS+ system and accompanying Image Lab software (Bio-Rad Laboratories). Cell fractionation experiments were carried out as previously described (Behrmann et al., 2004). Details on immunoprecipitation can be found in the Extended Experimental Procedures.

ECIS

HUVECs, passages 4–6, were cultured in MCDB-131 (VEC Technologies) with the addition of 10% fetal bovine serum (Omega Scientific) that was stripped using 0.25% dextran-coated charcoal (Sigma). PR-infected HUVECS were seeded onto 8W10E+ arrays and treated with P4 (100 nM) after cells reached confluence (Applied Biophysics). Data were acquired and analyzed using ECIS software (Applied Biophysics). For details on the reagents used in the ECIS experiments, see the Extended Experimental Procedures.

ChIP and Library Preparation

For each condition (negative control, PR+P4, PR only, and IgG control) 10 × 10^6 and 2 × 10^6 cultured HUVECs were used per IP for ChIP-seq and ChIP-qPCR, respectively. HUVECs were infected with a PR lentivirus, grown to confluence, and then treated with P4 for 1 hr. The library for sequencing was constructed using the Ovation Ultralow IL Multiplex System 1-8 (Nugen) according to the manufacturer's instructions. Libraries were sequenced using HIseq-2000 (Illumina) to obtain 50 bp long reads. The ChIP-seq data sets have been deposited in the National Center for Biotechnology Information (NCBI) Gene Expression Omnibus (GEO) under accession number GSE43786. For details on ChIP and how peaks were called and analyzed, see the Extended Experimental Procedures.

RNA Isolation, qPCR, and Library Preparation

Total RNA was extracted from organs and cells using the RNeasy Kit (QIAGEN), cDNA generated using the SuperScript First-strand Synthesis System (Invitrogen), and real-time qPCR was performed using SYBR Green reagent (QIAGEN) and detected using an Opticon2 PCR machine (MJ Research; BioRad). The library for sequencing was constructed using the Illumina Multiplex System (Illumina) according to the manufacturer's instructions. Libraries were sequenced using HIseq-2000 (Illumina) to obtain 50-bp-long reads. The RNA-seq data sets have been deposited in the NCBI GEO under accession number GSE46502. For details on how differentially expressed genes were identified and analyzed see the Extended Experimental Procedures.

Statistical Analysis

For statistical analysis, Student's unpaired two-tailed t test was used for all comparisons.

ACCESSION NUMBERS

The ChIP-seq and RNA-seq data sets have been deposited in the NCBI GEO under accession numbers GSE43786 and GSE46502, respectively.

SUPPLEMENTAL INFORMATION

Supplemental Information includes Extended Experimental Procedures, seven figures, and two tables and can be found with this article online at http://dx.doi.org/10.1016/j.cell.2013.12.025.

REFERENCES

Arnal, J.F., Fontaine, C., Billon-Galés, A., Favre, J., Laurell, H., Lenfant, F., and Gourdy, P. (2010). Estrogen receptors and endothelium. Arterioscler. Thromb. Vasc. Biol. 30, 1506–1512.

Atkins, G.B., Jain, M.K., and Hamik, A. (2011). Endothelial differentiation: molecular mechanisms of specification and heterogeneity. Arterioscler. Thromb. Vasc. Biol. 31, 1476–1484.

Behrmann, I., Smyczek, T., Heinrich, P.C., Schmitz-Van de Leur, H., Komyod, W., Giese, B., Müller-Newen, G., Haan, S., and Haan, C. (2004). Janus kinase (Jak) subcellular localization revisited: the exclusive membrane localization of endogenous Janus kinase 1 by cytokine receptor interaction uncovers the Jak.receptor complex to be equivalent to a receptor tyrosine kinase. J. Biol. Chem. 279, 35486–35493.

Bernelot Moens, S.J., Schnitzler, G.R., Nickerson, M., Guo, H., Ueda, K., Lu, Q., Aronovitz, M.J., Nickerson, H., Baur, W.E., Hansen, U., et al. (2012). Rapid estrogen receptor signaling is essential for the protective effects of estrogen against vascular injury. Circulation 126, 1993–2004.

Chappell, J.C., and Bautch, V.L. (2010). Vascular development: genetic mechanisms and links to vascular disease. Curr. Top. Dev. Biol. 90, 43–72.

Das, A., Mantena, S.R., Kannan, A., Evans, D.B., Bagchi, M.K., and Bagchi, I.C. (2009). De novo synthesis of estrogen in pregnant uterus is critical for stromal decidualization and angiogenesis. Proc. Natl. Acad. Sci. USA 106, 12542–12547.

Dejana, E., Orsenigo, F., and Lampugnani, M.G. (2008). The role of adherens junctions and VE-cadherin in the control of vascular permeability. J. Cell Sci. 121, 2115–2122.

Dvorak, H.F. (2010). Vascular permeability to plasma, plasma proteins, and cells: an update. Curr. Opin. Hematol. 17, 225–229.

Edwards, D.P., Altmann, M., DeMarzo, A., Zhang, Y., Weigel, N.L., and Beck, C.A. (1995). Progesterone receptor and the mechanism of action of progesterone antagonists. J. Steroid Biochem. Mol. Biol. 53, 449–458.

Fan, X., Krieg, S., Kuo, C.J., Wiegand, S.J., Rabinovitch, M., Druzin, M.L., Brenner, R.M., Giudice, L.C., and Nayak, N.R. (2008). VEGF blockade inhibits angiogenesis and reepithelialization of endometrium. FASEB J. 22, 3571–3580.

Franco, H.L., Rubel, C.A., Large, M.J., Wetendorf, M., Fernandez-Valdivia, R., Jeong, J.-W., Spencer, T.E., Behringer, R.R., Lydon, J.P., and Demayo, F.J. (2012). Epithelial progesterone receptor exhibits pleiotropic roles in uterine development and function. FASEB J. *26*, 1218–1227.

Gellersen, B., Brosens, I.A., and Brosens, J.J. (2007). Decidualization of the human endometrium: mechanisms, functions, and clinical perspectives. Semin. Reprod. Med. *25*, 445–453.

Hickey, M., and Fraser, I.S. (2002). Surface vascularization and endometrial appearance in women with menorrhagia or using levonorgestrel contraceptive implants. Implications for the mechanisms of breakthrough bleeding. Hum. Reprod. *17*, 2428–2434.

Huang, W., Sherman, B.T., and Lempicki, R.A. (2009). Bioinformatics enrichment tools: paths toward the comprehensive functional analysis of large gene lists. Nucleic Acids Res. *37*, 1–13.

Hyder, S.M., Stancel, G.M., Chiappetta, C., Murthy, L., Boettger-Tong, H.L., and Makela, S. (1996). Uterine expression of vascular endothelial growth factor is increased by estradiol and tamoxifen. Cancer Res. *56*, 3954–3960.

Iafrati, M.D., Karas, R.H., Aronovitz, M., Kim, S., Sullivan, T.R., Jr., Lubahn, D.B., O'Donnell, T.F., Jr., Korach, K.S., and Mendelsohn, M.E. (1997). Estrogen inhibits the vascular injury response in estrogen receptor alpha-deficient mice. Nat. Med. *3*, 545–548.

Ismail, P.M., Li, J., DeMayo, F.J., O'Malley, B.W., and Lydon, J.P. (2002). A novel LacZ reporter mouse reveals complex regulation of the progesterone receptor promoter during mammary gland development. Mol. Endocrinol. *16*, 2475–2489.

Strauss, J.F., and Barbieri, R.L. (2009). Yen and Jaffe's Reproductive Endocrinology (Amsterdam: Elsevier Health Sciences).

Kim, K.H., and Bender, J.R. (2009). Membrane-initiated actions of estrogen on the endothelium. Mol. Cell. Endocrinol. *308*, 3–8.

Komarova, Y., and Malik, A.B. (2010). Regulation of endothelial permeability via paracellular and transcellular transport pathways. Annu. Rev. Physiol. *72*, 463–493.

Kovacs, G. (1996). Progestogen-only pills and bleeding disturbances. Hum. Reprod. *11* (*Suppl 2*), 20–23.

Krikun, G., Schatz, F., Taylor, R., Critchley, H.O.D., Rogers, P.A.W., Huang, J., and Lockwood, C.J. (2005). Endometrial endothelial cell steroid receptor expression and steroid effects on gene expression. J. Clin. Endocrinol. Metab. *90*, 1812–1818.

Large, M.J., and DeMayo, F.J. (2012). The regulation of embryo implantation and endometrial decidualization by progesterone receptor signaling. Mol. Cell. Endocrinol. *358*, 155–165.

Lydon, J.P., DeMayo, F.J., Funk, C.R., Mani, S.K., Hughes, A.R., Montgomery, C.A., Jr., Shyamala, G., Conneely, O.M., and O'Malley, B.W. (1995). Mice lacking progesterone receptor exhibit pleiotropic reproductive abnormalities. Genes Dev. *9*, 2266–2278.

Lydon, J.P., DeMayo, F.J., Conneely, O.M., and O'Malley, B.W. (1996). Reproductive phenotpes of the progesterone receptor null mutant mouse. J. Steroid Biochem. Mol. Biol. *56* (1-6 Spec No), 67–77.

Maybin, J.A., and Duncan, W.C. (2004). The human corpus luteum: which cells have progesterone receptors? Reproduction *128*, 423–431.

McKenna, N.J., and O'Malley, B.W. (2000). From ligand to response: generating diversity in nuclear receptor coregulator function. J. Steroid Biochem. Mol. Biol. *74*, 351–356.

Orsenigo, F., Giampietro, C., Ferrari, A., Corada, M., Galaup, A., Sigismund, S., Ristagno, G., Maddaluno, L., Koh, G.Y., Franco, D., et al. (2012). Phosphorylation of VE-cadherin is modulated by haemodynamic forces and contributes to the regulation of vascular permeability in vivo. Nat. Commun. *3*, 1208.

Pearen, M.A., and Muscat, G.E.O. (2010). Minireview: Nuclear hormone receptor 4A signaling: implications for metabolic disease. Mol. Endocrinol. *24*, 1891–1903.

Pei, L., Castrillo, A., and Tontonoz, P. (2006). Regulation of macrophage inflammatory gene expression by the orphan nuclear receptor Nur77. Mol. Endocrinol. *20*, 786–794.

Perrot-Applanat, M., Cohen-Solal, K., Milgrom, E., and Finet, M. (1995). Progesterone receptor expression in human saphenous veins. Circulation *92*, 2975–2983.

Regan, E.R., and Aird, W.C. (2012). Dynamical systems approach to endothelial heterogeneity. Circ. Res. *111*, 110–130.

Rubel, C.A., Lanz, R.B., Kommagani, R., Franco, H.L., Lydon, J.P., and DeMayo, F.J. (2012). Research resource: genome-wide profiling of progesterone receptor binding in the mouse uterus. Mol. Endocrinol. *26*, 1428–1442.

Runic, R., Schatz, F., Wan, L., Demopoulos, R., Krikun, G., and Lockwood, C.J. (2000). Effects of norplant on endometrial tissue factor expression and blood vessel structure. J. Clin. Endocrinol. Metab. *85*, 3853–3859.

Shifren, J.L., Tseng, J.F., Zaloudek, C.J., Ryan, I.P., Meng, Y.G., Ferrara, N., Jaffe, R.B., and Taylor, R.N. (1996). Ovarian steroid regulation of vascular endothelial growth factor in the human endometrium: implications for angiogenesis during the menstrual cycle and in the pathogenesis of endometriosis. J. Clin. Endocrinol. Metab. *81*, 3112–3118.

Shoupe, D., Mishell, D.R., Jr., Bopp, B.L., and Fielding, M. (1991). The significance of bleeding patterns in Norplant implant users. Obstet. Gynecol. *77*, 256–260.

Sugino, N., Kashida, S., Karube-Harada, A., Takiguchi, S., and Kato, H. (2002). Expression of vascular endothelial growth factor (VEGF) and its receptors in human endometrium throughout the menstrual cycle and in early pregnancy. Reproduction *123*, 379–387.

Vázquez, F., Rodríguez-Manzaneque, J.C., Lydon, J.P., Edwards, D.P., O'Malley, B.W., and Iruela-Arispe, M.L. (1999). Progesterone regulates proliferation of endothelial cells. J. Biol. Chem. *274*, 2185–2192.

Wetendorf, M., and DeMayo, F.J. (2012). The progesterone receptor regulates implantation, decidualization, and glandular development via a complex paracrine signaling network. Mol. Cell. Endocrinol. *357*, 108–118.

Zhao, Y., and Bruemmer, D. (2010). NR4A orphan nuclear receptors: transcriptional regulators of gene expression in metabolism and vascular biology. Arterioscler. Thromb. Vasc. Biol. *30*, 1535–1541.

Zhao, D., Qin, L., Bourbon, P.M., James, L., Dvorak, H.F., and Zeng, H. (2011). Orphan nuclear transcription factor TR3/Nur77 regulates microvessel permeability by targeting endothelial nitric oxide synthase and destabilizing endothelial junctions. Proc. Natl. Acad. Sci. USA *108*, 12066–12071.

Zhu, Y., Bian, Z., Lu, P., Karas, R.H., Bao, L., Cox, D., Hodgin, J., Shaul, P.W., Thoren, P., Smithies, O., et al. (2002). Abnormal vascular function and hypertension in mice deficient in estrogen receptor beta. Science *295*, 505–508.